Materials and Design 36 (2012) 415–420

Contents lists available at SciVerse ScienceDirect

Materials and Design

journal homepage: www.elsevier.com/locate/matdes

Technical Report

Simulation of induction tempering process of carbon steel using finite element method

A. Zabett, S.H. Mohamadi Azghandi *

Department of Metallurgical and Materials Engineering, Faculty of Engineering, Ferdowsi University of Mashhad, Mashhad 91677-1111, Iran

ARTICLE INFO

Article history:
Received 18 September 2011
Accepted 29 October 2011
Available online 6 November 2011

ABSTRACT

A numerical model was developed to simulate an induction tempering process, solving an electromagnetic-thermal coupled problem. The temperature distribution inside an alloy steel work-piece was computed and the final hardness was predicted using Jaffe and Gordon relation. The experiments were undertaken with different induction process settings at some industrial conditions. The effects of induction parameters i.e. input AC current density, coil velocity and coil stay time were investigated by employing the proposed model and the results were compared to the experimental data. The computed results are in a good agreement with the experimental data. As an example, the model predicted the final hardness at three given points 47, 45 and 37 HRC. For this tempering condition the experimental results were 51, 45 and 36 HRC, respectively.

1. Introduction

Extensive production experience has implicated the commercial success of induction tempering for many applications. Regarding the influence of induction parameters on the final hardness of tempered work-piece, the ability to predict these effects could be very helpful. The simulation of tempering process provides appropriate tool to study important process parameters. Simulation of such processes is usually very complex and involves numerical solving of electromagnetic field coupled to heat transfer problem. It consists of three main parts; heating, cooling and hardening.

There have been many efforts to simulate induction processes, to predict metallurgical aspects and to investigate the effects of parameters by means of numerical analysis and experimental tests. The earlier work, Wang et al. [1] simulated induction hardening process, using FEM. In another work, they simulated induction hardening process with a moving coil [2]. The previous researches are resulted in thermal history of the work-piece through induction heating. Sadeghipour et al. proposed a computer based FEM model to simulate induction hardening process [3]. The effects of solving parameters such as time step were studied in this work. In the next step, researchers [4–7] predicted final hardness and microstructure of induction-hardened work-pieces by simulating the process. Cajnera et al. [4] predicted the hardening depth and the surface hardness after induction tempering which depicted a good conformity with the experimental data. Yuan et al. [6] studied the modeling of phase transformation during induction hardening and estimated the hardness based on volume fraction of produced phases. Magnabosco et al. [8] investigated induction hardening process of C45 steel bar numerically to predict hardness and microstructure and they tested the process to validate the numerical results claimed satisfactory agreement.

Kristoffersen and Vomacka [9] and Kayacan and Colak [10] studied the effects of induction parameters such as frequency, coil shape and applied current on final microstructure and the hardness of the work-pieces. Coupard et al. [11] and Kim and Na [12] computed the residual stresses for inductively surface hardened steels. However, few researches have focused on induction tempering process. Ahn et al. [13] investigated microstructure evolution and mechanical properties of low alloy steel tempered by induction heating.

In the present study a steering pinion was used as the work-piece for the experiments (Fig. 1). The pinion is ranked as a safety auto part and must fulfill several quality requirements such as wear resistant, impact and fatigue resistant. For example, the spline and the thread regions are subjected to impact and torsion, therefore a relatively high toughness is expected for these regions while the shaft region should be surface hardened appropriately. The quality requirements are implicated by a restrict production procedure and a specific hardness profile through the work-piece.

The induction heating process which uses a moving coil to temper the hardened steering pinion was simulated using an integrated finite element analysis. Electromagnetic field analysis which produces Joule heat for heating stage and heat transfer analysis during the cooling stage due to calm air flow on the work-piece surface were carried out to obtain temperature distribution inside the work-piece. Final hardness was computed, using Jaffe and Gordon

* Corresponding author. Tel.: +98 5118763305; fax: +98 5118763301.
E-mail address: h.mohamadi@um.ac.ir (S.H. Mohamadi Azghandi).

0261-3069/$ - see front matter © 2011 Published by Elsevier Ltd.
doi:10.1016/j.matdes.2011.10.052

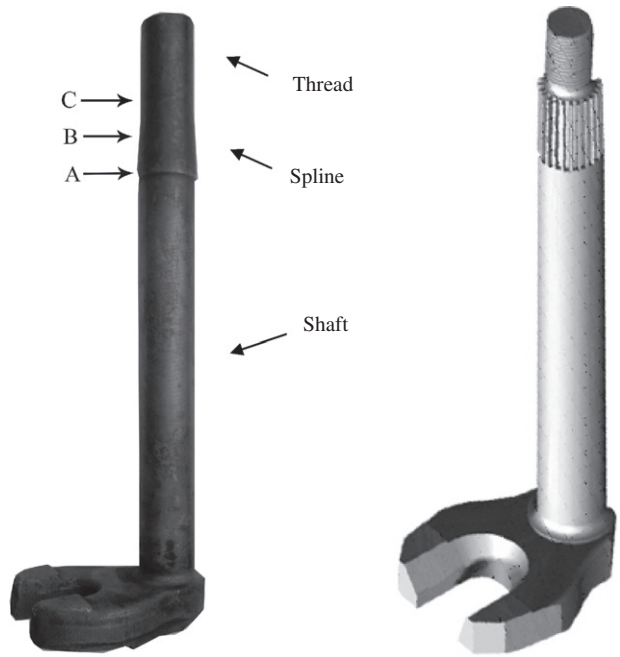

Fig. 1. Steering pinion before and after finishing. Points A, B and C are the locations of the hardness measurement.

equation [14]. Influences of the induction parameters, i.e. primary coil stay time, coil velocity and input AC current density were also investigated by using the developed model and doing the experiments at industrial condition.

2. Experimental procedure

The steering pinion is made of AISI 4130 steel with the chemical composition shown in Table 1. Heat treatment process comprises of carburizing and tempering. The pinion is carburized at 920 °C for 8 h in a controlled atmosphere furnace and then oil quenched. The splines and threads regions are inductively tempered. The induction tempering process begins with the coil set at the point A of the splines section (see Fig. 1). Applying AC current, the coil stays for a specific time, t_1, referred to as primary stay time. The coil moves along the splines section with the velocity (V_1) and moves over the threads region with a different velocity (V_2). The coil is kept for a given time, t_2, at the end of the process while the AC current is on. The induction heating program is shown in Fig. 2.

The main parameters affecting the tempering process include electrical current density, frequency, primary stay time, final stay time, coil velocity along the splines section, coil velocity along the threads section and the air gap between the work-piece and the coil. The frequency and the air gap are fixed. Since the aim of this work is the prediction of the hardness at the splines section, the velocity across the threads section and the final stay time have little effects on the results. Therefore, the effective parameters considered here are the AC current density, the initial stay time and the velocity over the splines section. The induction parameters used for different tempering conditions are shown in Table 2.

Table 1
Chemical composition of AISI 4130 steel.

Element	C	Mn	Si	Cr	Mo	S	P	Ni	Cu
wt pct	0.19	0.74	0.24	0.92	0.18	0.003	0.007	0.08	0.16

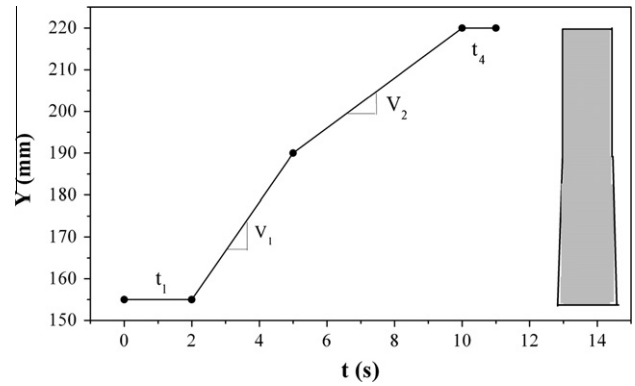

Fig. 2. Schematic coil movement along the pinion.

Table 2
Induction parameters for experimental conditions.

Induction condition	D.A (10^7 A/m^2)	F (kHz)	t_0 (s)	t_f (s)	V_1 (mm/s)	V_2 (mm/s)	Air gap (mm)
I	2.5	30	1.7	0.7	11	7	4
II	2.5	30	1.7	0.7	9.2	7	4
III	2.5	30	2.2	0.7	11	7	4
IV	2.8	30	1.7	0.7	11	7	4

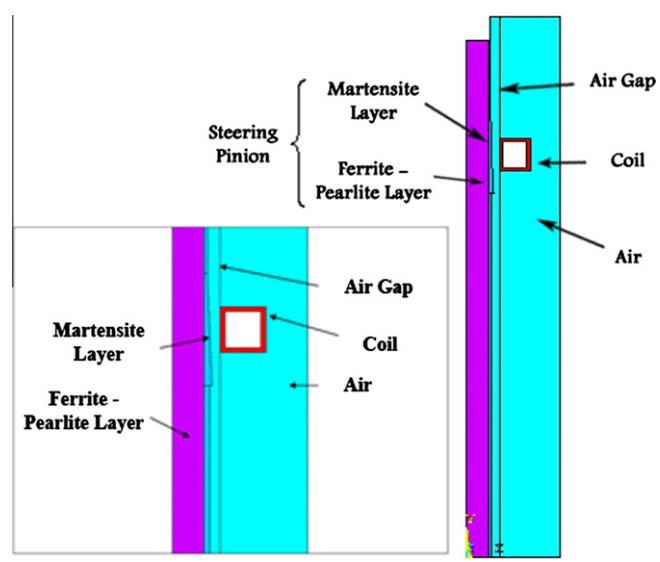

Fig. 3. Schematic picture of the model components.

3. Modeling

The modeling in this study comprises of the electromagnetic-thermal coupled of induction tempering and predicting the hardness based on the computed temperatures.

3.1. Electromagnetic analysis

During the induction heating, AC current passing through the coil creates a magnetic field around the work-piece. The magnetic field induces a current in the surface layer of the work-piece and the electrical resistance causes the heat generation.

Magnetic vector potential is expressed by [15]

$$A = \frac{\mu_0 \cdot I}{4\pi} \int_s \frac{dl}{|r|} \tag{1}$$

where I, μ_0, l and r are the input AC current density to the induction coil, the magnetic permeability of vacuum, the coil circumference and the coil radius. According to Gauss' law the magnetic flux density B can be calculated:

$$B = \nabla \times A \tag{2}$$

Faraday's law expresses the electric field intensity E and the magnetic field intensity H by

$$\nabla \times E = -\frac{\partial B}{\partial t} \tag{3}$$

$$H = \frac{B}{\mu} \tag{4}$$

here μ is the magnetic permeability of the medium. Employing Ampere's circuit law, the induced current density inside the specimen J, is calculated by

$$J = \nabla \times H - \frac{\partial(\varepsilon \cdot E)}{\partial t} \tag{5}$$

and the amount of the heat generated by the eddy current Q is

$$Q_{induction} = \frac{J^2}{\sigma} \tag{6}$$

where ε and σ indicate the permittivity and the electrical conductivity of the work-piece.

3.2. Thermal analysis

The generated heat penetrates inside the work-piece radially and longitudinally. Using the heat transfer differential equation, the temperature distribution of the work-piece can be calculated. Three different heat transfer modes; conduction, convection and radiation were taken into account. The governing equations are [1,16]

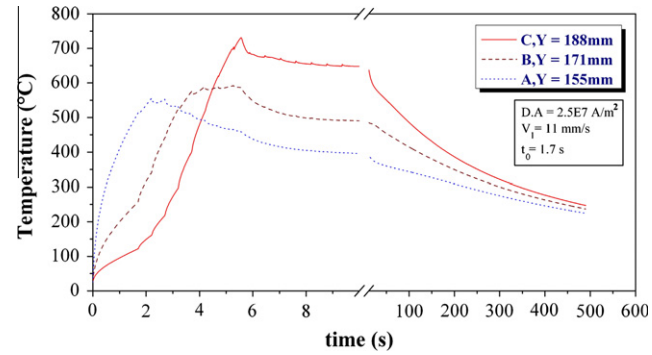

Fig. 5. Predicted temperature–time curves at three points A, B and C, condition I.

$$\rho C_p \frac{\partial T}{\partial t} = k \frac{\partial^2 T}{\partial x^2} + Q_{induction} \tag{7}$$

$$x = x_0 \quad -k \frac{\partial T}{\partial x} = h_{OV}(T - T_\infty) \tag{8}$$

$$h_{OV} = h_C + h_R \tag{9}$$

$$h_R = \sigma\varepsilon \left(\frac{T^4 - T_\infty^4}{T - T_\infty} \right) \tag{10}$$

where ρ, C_p and k are the density, specific heat capacity and thermal conductivity of the work-piece respectively. x_0 indicates the dis-

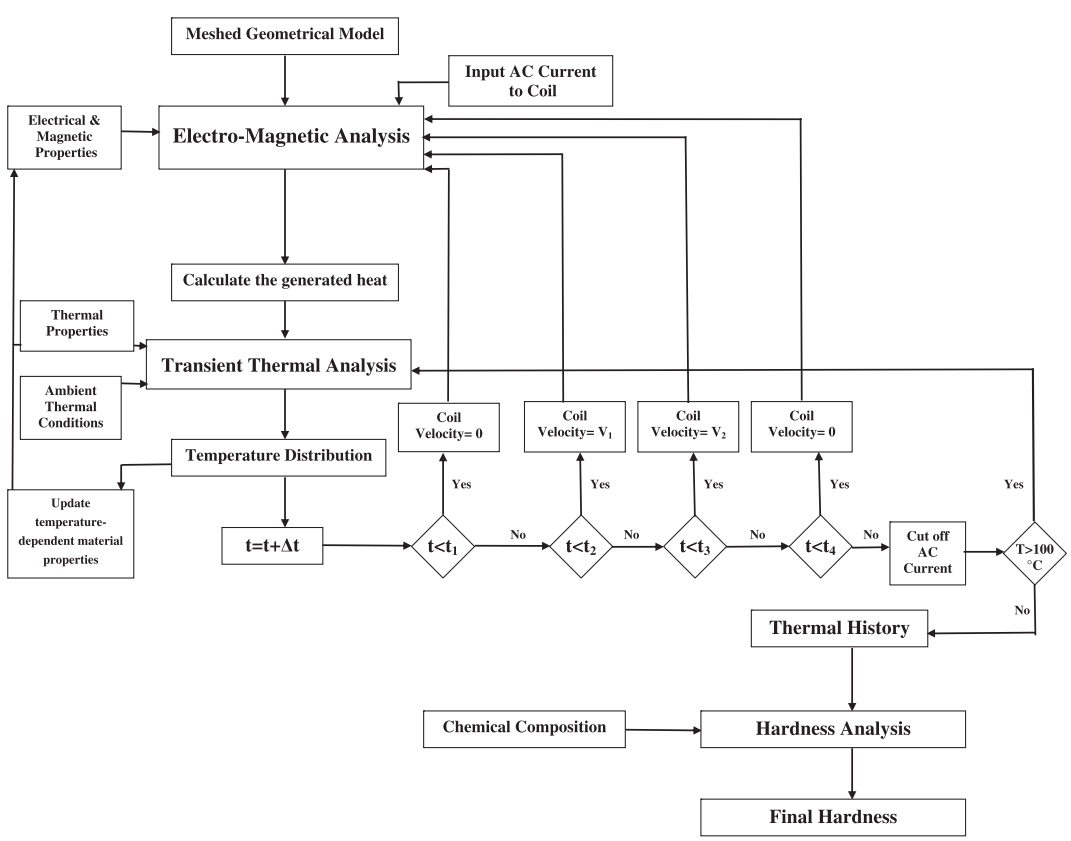

Fig. 4. Flow chart of the model; induction heating analysis and hardness analysis.

tance between the core and the surface of the work-piece. h_{OV}, h_C and h_R represent the overall heat transfer coefficient, the convection heat transfer coefficient and the radiation heat transfer coefficient. In Eq. (10), σ, ε and T_∞ are Boltzman constant, the emissivity coefficient and the ambient temperature respectively. The work-piece is air cooled by $h = 10\frac{w}{m^2}$ and $T_\infty = T_0 = 25\ ^\circ C$.

3.3. Finite element analysis

In this work, a powerful FEM package, ANSYS10 which contains solver algorithm for heat transfer and electromagnetic analysis equipped with distinctive algorithm due to solve couple analysis based on finite element method was applied to model the induction tempering process. In the mathematical model, temperature distribution is calculated according to electromagnetic properties while the electromagnetic properties depend on the temperature. To solve the nonlinear problem, a maximum iteration of 10,000 was considered. Finite element method was employed to solve two main differential Eqs. (5) and (7). In order to solve the mathematical problem, Newmark time integration method (including an improved algorithm called HHT) which are used for implicit transient analyses was employed. The 4-node quadratic element was selected to model the parts geometrically. Time step was chosen to be $\Delta t = 0.02$ s. In order to consider the movement of the coil, the total induction time was divided into n time-steps and the coil position was changed by every time-step. Every time-step contains m sub-steps. The physical model consists of four major parts; pinion, copper coil, air gap between the coil and the pinion and air environment around the coil. The pinion has been composed of two sections; the carburized layer with martensite microstructure and the ferrite–pearlite region (Fig. 3). Turning on the coil and moving it are resulted in producing eddy currents which are lead to generate the heat to warm up the work-piece. It causes to change the work-piece microstructure and eventually reduce the hardness. The air gap and air environment affect on the induced current because of magnetic permeability of air. Therefore they should be considered in the model. Mesh size is changed within the pinion radius. The surface mesh is finer than that of the core. The model was assumed to be 2 dimensional and axis-symmetrical. The thermal, electrical and magnetic properties of the steel depend on the temperature and the microstructure. These were accounted for in the model [17].

3.4. Hardness analysis

After the calculations of the temperature profile inside the work-piece Jaffe and Gordon model was used to predict the hardness. Jaffe and Gordon model expresses the hardness by [14]

$$T = 16.67(H_C - H_a) - 17.8 \tag{11}$$

In this relation the temperature is in degree Celsius and the hardness is in Rockwell C. T is the tempering temperature to achieve the required hardness (H_a) after 4 h of tempering. H_C is called the chemical hardness and can be defined by Eq. (12) [14].

$$H_C = H_{carbon} + H_{Alloying} + H_{G.S} \tag{12}$$

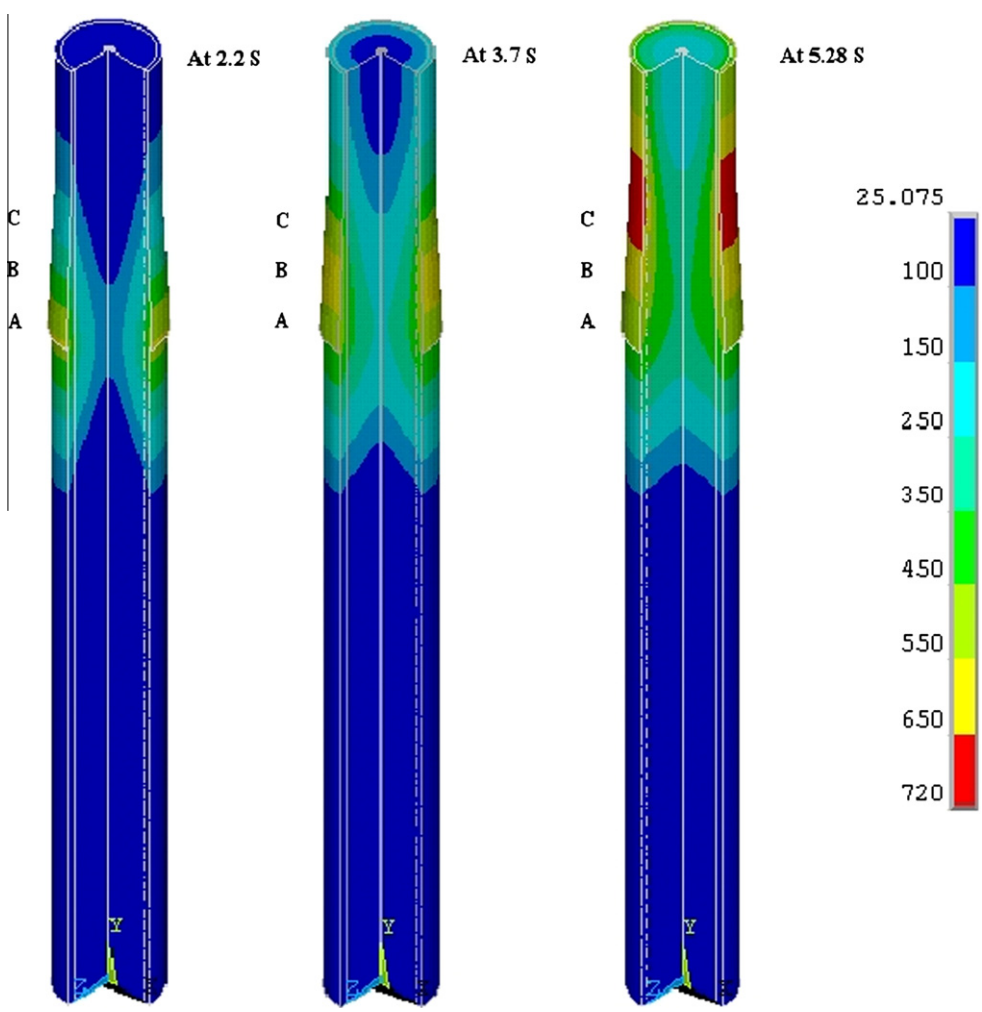

Fig. 6. Temperature distributions inside the work-piece for three different times, condition I.

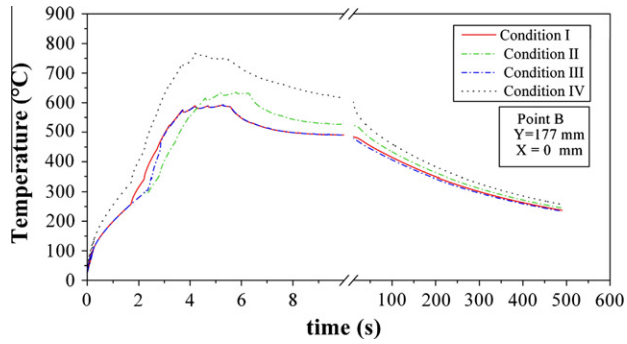

Fig. 7. Predicted temperature–time curves for different induction conditions, point B.

Here H_{carbon}, $H_{Alloying}$ and $H_{G.S}$ indicate the martensite hardness with a specific amount of carbon, hardness related to alloying elements and hardness related to grain size, respectively [14]. The grain size number based on ASTM E112-2004 [18] used in this study is 9. According to the chemical composition (Table 1) and ASTM grain size number, ($H_{Alloying} + H_{G.S}$) is calculated to be 5.1 HRC. Knowing H_C, one can solve for H_a at any given temperature or can predict the required temperature T, for any wanted tempering hardness H_a.

In order to find the tempering hardness at different holding time, the following logarithmic relation can be employed [19].

$$T_1(C + \log t_1) = T_2(C + \log t_2) \tag{13}$$

In Eq. (13), t is time in hour, T is temperature in Kelvin and C is a constant equal to 18. The maximum temperature reached during the processes plays an important role in estimation of the final hardness. Eq. (11) is suggested for an isothermal tempering process. In this study the temperature is not constant. However, Eq. (13) can be used to normalize the whole heat treatment history of the sample for any temperature. Therefore, an equivalent temperature can be found for any induction tempering practice which may be related to 4 h of isothermal tempering (according to Jaffe and Gordon relation). Fig. 4 reveals the flow chart of the model. In this flow chart t_1, t_2, t_3, t_4 are related to coil movement steps. Furthermore, since tempering temperature is usually considered upper than 100 °C, the stop creation of the model was chosen to be $T = 100$ °C.

4. Results and discussion

The simulated results consist of temperature–time profiles, temperature distribution contours and final hardness profiles.

As it can be seen in Fig. 5, the calculated maximum temperature at points A ($Y = 155$ mm), B ($Y = 171$ mm) and C ($Y = 188$ mm) are 555, 592 and 731 °C respectively. It reveals a difference of 176 °C between the maximum temperature of the point A and that of the point C. Furthermore, the duration time at elevated temperatures for the point C is much more than that of the point A. For the point C, the duration time that the temperature is higher than 500 °C is about 95 s while it is just about 2 s for the point A. It is well expected for the point C to have lower hardness that of the point A.

In order to verify the results, the maximum temperature of the point C was measured by an infrared thermometer (ULTIMAX UX20) to be 710 °C. Due to some restrictions, such as small working space, moving parts and on site calibration difficulties, some measurement error is expected. Nevertheless, the simulated temperature (731 °C) is close enough to the measured temperature (710 °C).

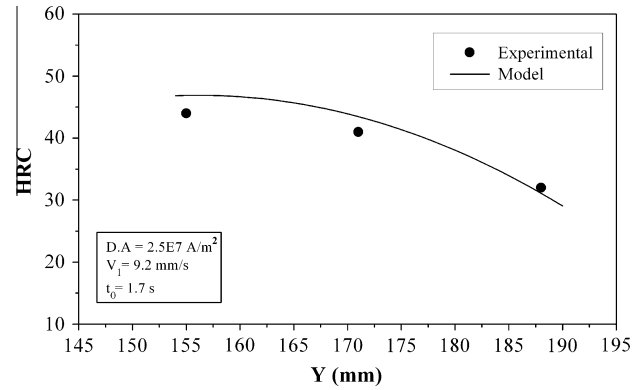

Fig. 8. Experimental results and predicted surface hardness along the work-piece, condition II.

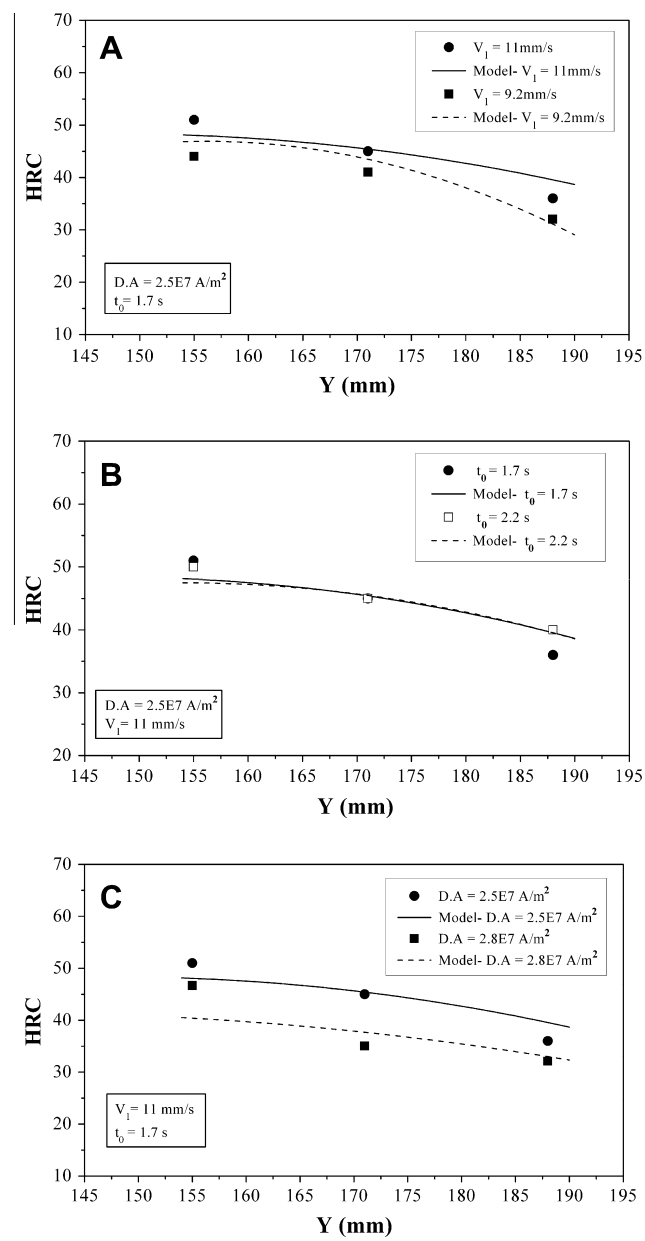

Fig. 9. Experimental results and predicted surface hardness along the work-piece, (a) conditions I & II (b) conditions I & III (c) conditions I & IV.

Fig. 6 shows temperature distributions of the work-piece for condition I. At the beginning, the surface temperature is higher than that of the core and the thermal gradient from the surface into the specimen is steep while it is reduced through time. Using the model the position of the maximum temperature could be readily distinguished and the temperature profile and the thermal history can be easily studied.

Temperature–time variations for four different induction conditions were studied. As it can be seen in Fig. 7, the temperature profile shifted into higher levels when the induction condition was changed from I to II (decreasing the coil velocity) and from I to IV (increasing the applied AC current). Changing the coil stay time did not influence the temperature profile (compare condition I to condition III).

Fig. 8 shows the results of predicted hardness by the model for condition II and compares them with the experimental data. The maximum deviation at point A (Y = 155 mm) is 6% and the average deviation is about 4.6%.

Fig. 9 shows the results of the model and the experiments for conditions I, II, III and IV. Good agreement of the experimental results with the computed hardness can be seen in this figure. Fig. 9 also compares the effects of induction parameters. Fig. 9a illustrates the effect of velocity on the hardness profile comparing condition I to condition II. Fig. 9b shows the indifference between the results of condition I to those of condition III. In other word, little effect of initial stay time on the hardness of the spline section can be concluded. In Fig. 9c the role of the most effective induction parameter on the hardness of the spline section can be seen. An increase of AC current density from 2.5×10^7 to 2.8×10^7 A/m^2 leads to an average hardness reduction of about 6 HRC at the spline section. Comparison with Jaffe and Gordon model [14], the proposed hardness predictor model was developed to estimate the hardness after non-isothermal tempering such as induction tempering process while the previous model [14] was only able to predict the hardness after isothermal tempering process.

5. Conclusions

The proposed model is able to predict the hardness of carbon steel work-piece after induction tempering process and using the model, it is possible to study the thermal history of the work-piece through the process.

The experimental results verified the predictions and the computed results are in a good agreement with the experimental data, 5% error approximately.

This model can be used to study the effects of induction parameter and can be used to find the initial setting for any similar induction tempering process to reach the surface hardness required for the work-piece. Study of three main induction parameters namely, input AC current density, coil velocity and coil stay time showed that AC current density was the most effective parameter. A change of current density from 2.5×10^7 to 2.8×10^7 A/m^2 led to an average hardness reduction of about 6 HRC at the spline section. Additionally, decreasing the Coil velocity (V_1) from 11 to 9.2 mm/s resulted in an average reduction of 3 HRC.

References

[1] Wang KF, Chandrasekar S, Yang HTY. Finite-element simulation of induction heat treatment. J Mater Eng Perform 1992;1:97–112.
[2] Wang KE, Chandrasekar S, Yang HTY. Finite-element simulation of moving induction heat treatment. J J Mater Eng Perform 1995;4:460–73.
[3] Sadeghipour K, Dopkin JA, Li K. A computer aided finite element/experimental analysis of induction heating process of steel. Comput Ind 1996;28:195–205.
[4] Cajnera F, Smoljan B, Landek D. Computer simulation of induction hardening. J Mater Process Tech 2004;157–158:55–60.
[5] Dietmar H. A mathematical model for induction hardening including mechanical effects. Nonlinear Anal-Real 2004;5:55–90.
[6] Yuan J, Kang J, Rong Y, Sisson RD. FEM modeling of induction hardening processes in steel. J Mater Eng Perform 2003;12:589–96.
[7] Dolezel I, Barglik J, Ulrych B. Continual induction hardening of axi-symmetric bodies. J Mater Process Tech 2005;161:269–75.
[8] Magnabosco I, Ferro P, Tiziani A, Bonollo F. Induction heat treatment of a ISO C45 steel bar: Experimental and numerical analysis. Comp Mater Sci 2006;35:98–106.
[9] Kristoffersen H, Vomacka P. Influence of process parameters for induction hardening on residual stresses. Mater Design 2001;22:637–44.
[10] Kayacan MC, Colak O. A fuzzy approach for induction hardening parameters selection. Mater Design 2004;25:155–61.
[11] Coupard D, Palin-luc T, Bristiel P, Ji V, Dumas C. Residual stresses in surface induction hardening of steels: Comparison between experiment and simulation. Mater Sci Eng A 2008;487:328–39.
[12] Kim WB, Na SJ. A study on residual stresses in surface hardening by high frequency induction heating. Surf Coat Tech 1992;52:281–8.
[13] Ahn ST, Kim DS, Nam WJ. Microstructural evolution and mechanical properties of low alloy steel tempered by induction heating. J Mater Process Tech 2005;160:54–8.
[14] Thelning KE. Steel and its heat treatment. 2nd ed. Great Britain: Mackays of Chatham; 1984.
[15] Sturgess JP, Preston TW. An economic solution for 3D coupled electromagnetic and thermal eddy current problems. IEEE T Magn 1992;28:1267–9.
[16] Campbell PC, Hawbolt EB, Brimacombe JK. Microstructure engineering applied to controlled cooling of steel wire rode: part 1. Experimental design and heat transfer. Metall Mater Trans A 1991;22:2769–78.
[17] ASM Handbook, vol. 1, Properties and selection: Irons, steels and high performance alloys, 2nd ed. Materials Park, OH: ASM International; 2004.
[18] Annual book of ASTM Standard, vol. 3.01. E0112-10 Test methods for determining average grain size, ASTM Philadelphia; 2011.
[19] ASM Handbook, vol. 4. Heat treating, 2nd ed. Materials Park, OH: ASM International; 2004.